Estimation of SOH Degradation of Coin Cells Subjected to Accelerated Life Cycling with Randomized Cycling Depths and C-Rates

Pradeep Lall[(1)], Ved Soni[(1)], Guneet Sethi[(2)], Kok Yiang[(2)]
[(1)]NSF-CAVE3 Electronics Research Center,
Department of Mechanical Engineering,
Auburn University, Auburn, AL, 36849.
Email – lall@auburn.edu

[(2)]Amazon Lab 126,
Sunnyvale, CA.

***Abstract* - Investigation of li-ion battery state of health (SOH) degradation and its modeling facilitates determination of device warranty and can provide information about the device battery health. For such studies, batteries undergo life-cycling tests with fixed cycling depths and charging currents (C-rates) across cycles, and the gathered degradation data is used for model development. However, in the real world, the cycling depth is hardly constant per cycle and varies across users; the SOH estimation of such use-cases is challenging for lab-developed models. In this study, a semi-empirical SOH estimation regression model has been trained using fixed cycling depth and c-rate data and is validated using tests with randomized cycling depth and c-rate variation per cycle. Different upper and lower state of charge (SOC) limits were chosen to simulate different use profiles. Finally, multiple iterations of this model with different predictor variables have been tested to minimize the estimation error.**

***Index Terms* – capacity degradation, SOH modeling, SOH estimation, li-ion battery, randomized battery testing**

I. INTRODUCTION

The development of several flexible and portable consumer electronics products has increased interest in flexible electronics technology, especially flexible batteries. Flexible power sources have gained popularity outside of consumer electronics products, including roll-up screens, RFID tags, wearable sensors, and on-body biomedical devices [1][2][3]. When compared to other electrical energy storage (EES) technologies, lithium ion batteries (LIBs) offer a superior combination of specific energy and specific capacity (i.e., amount of charge supplied per unit weight) [4][5][6]. Additionally, LIBs also feature a long cycle life, ubiquity, high roundtrip efficiency, low maintenance requirements, choice of chemistries for specialized applications, low self-discharge rates, and long-term reliability [7].

Two prime objectives of lithium-ion battery degradation research are the identification of electrochemical failure modes of batteries in order to optimize battery design and developing techniques to estimate battery capacity degradation to determine its end-of-life (EOL), known as battery health prognostics. Battery prognostics primarily focuses on two issues: the first is estimating the state of health (SOH) of a battery to determine its state of capacity fade at a specific point in its life (SOH estimation) (see (1) [8]), and the second is predicting how long the battery will last given its current SOH (RUL prediction). The industry-accepted failure limit for li-ion batteries used in electronic devices is 80% SOH, i.e., the battery SOH has 20% points to go through (from 100% to 80%) until the battery is declared as failed [8]. Hence, the task of accurate SOH estimation is important in order to inform the user of current battery health and to detect impending battery failure within these 20% points.

$$\text{State of Health (SOH)} = \frac{\text{Battery Capacity}}{\text{Rated Capacity}} * 100 \quad (1)$$

Extensive testing of battery samples, followed by data processing and incorporation into various modeling frameworks, such as electrochemistry-based models, battery equivalent circuit models (ECM), or data-driven models, are required for the development of such SOH estimation and RUL prediction models [8]. Electrochemical modelling of batteries is challenging owing to its heavy reliance on the complex underlying electrochemomechanical battery physics, whereas equivalent circuit modeling requires usage of expensive testing equipment such as electrochemical impedance spectroscopy (EIS). The data-driven modeling approach involves accelerated life cycling of battery samples considering various use-parameters, including charge and discharge currents, operating temperature, depth of cycling, etc. which can be achieved using battery testing setups. The data produced during these tests is subsequently analyzed and related to the battery SOH using a variety of modeling techniques, including machine learning and regression modeling. Thus, the data-driven SOH and RUL estimation models are often preferred due to their relative simplicity and low cost.

Accordingly, many articles have been published in the past two decades documenting SOH degradation and various SOH estimation and RUL prediction models [8]. However, in most of these studies, accelerated life cycling with predetermined state of charge (SOC) bounds as well as fixed charge currents (C-rates) for each cycle is used while testing. However, in the real world, products using rechargeable batteries are frequently cycled with arbitrary SOC bounds. Hence, this testing approach does not accurately reflect real-world use case circumstances. Additionally, the models created using these data are frequently tested on datasets with

the same properties as the training data, such as fixed depth of cycling (DOC) and C-rates. Since the model isn't evaluated on randomized cycling/charging datasets, which are typical in the real-world scenarios, the model accuracy reported in such studies can frequently be deceptive. There are few studies that concentrate on testing and modeling for randomized cycling and charging, and those that do so frequently use machine learning-based SOH estimation models which are computationally taxing and require considerable amounts of device memory, making them challenging to be utilized in portable electronic devices where power and memory are limited for background operations.

The NASA dataset for random walk battery cycling is used by the majority of articles demonstrating SOH estimation techniques for randomized cycling [9]. Using indirect health indicators like battery voltage and current during accelerated life cycling, Yu [10] suggested an indirect SOH estimation approach relating the battery internal resistance to SOH degradation. The mean absolute error (MAE) of the elastic net model used is 2%. However, since only two battery sample datasets are used for model training, its robustness for SOH estimation may suffer. Additionally, it is challenging to accurately detect variables like internal resistance in portable electronic devices since it requires additional circuitry and specific charge-discharge profiles.

For randomized testing SOH estimation, Venugopal [11] used an independent recurrent neural network (RNN) with operating temperature, current, and battery voltage as input variables. The absolute error for this model has a maximum value of 2.59% and an average value of 1.14%. Only three datasets are used to create this model as well. Furthermore, Tian [12] utilized a different machine learning technique called the online sequential extreme learning machine (OSELM), and he claimed an MAE of 1%. The three features—discharge duration, voltage bounce-back after discharge, and variance of the randomized cycling voltage curve—that were extracted from the input data and utilized for model training would necessitate collecting a lot of data while the battery was in use.

Yang [13] combined a convolutional neural network (CNN) with a random forest machine learning technique. The partial training data used in this study was obtained by truncating full charge-discharge cycling data within predetermined SOC limits; therefore, it is not truly a randomized cycling dataset because the voltage and current profiles in a randomized cycling scenario and a deep cycling scenario are very different from one another. Depending on the battery data's maximum depth of cycling, they reported a SOH estimation MAE of 1–3%.

The goal of the current study is to fix some of the issues with the earlier research. This work proposes a semi-empirical nonlinear regression model for SOH estimation, which has been developed considering input variables derived from the battery voltage, current and operating temperature. The uniqueness of the developed model is that, it uses SOH degradation data generated from accelerated life cycling tests with fixed cycling depth limits and charge currents across various cycles, however, it performs SOH estimation of battery samples subjected to cycle-wise randomized cycling depth and randomized charging current tests. The model uses 32 training datasets consisting of two types of coin cells subjected varying C-rates, operating temperatures, depths of charge and depths of discharge per test. The generated nonlinear regression model was tested using 24 randomized cycling test datasets with varying upper and lower bounds of the state of charge within which the battery was cycled randomly; 6 more testing datasets with fixed cycling depth but varying charge C-rate per cycle; and 24 test datasets with both the cycling depth and C-rate randomized per cycle. Since the two coin cells used as test vehicles have different capacities, two model types were developed: one with the battery capacity as a variable (capacity conscious), and the second without (capacity agnostic). Furthermore, four model variants with differing input variables were developed for each model type to minimize the estimation error. For each model variant, six sub-variants were developed with the input training data sampled at different intervals to reduce the computational intensiveness of the SOH estimation process.

II. EXPERIMENTAL METHODOLOGY

A. *Test Vehicle*

As test vehicles for the current investigation, two commercially available coin cells from the same manufacturer were used: cell A (90 mAh) and cell B (120 mAh) [14]. Both cells shared the same cathode-anode chemistry (LiNiMnCoO2 (NMC) - graphite) and charge-discharge properties. The electrochemical characteristics of both cells are summarized in TABLE I:

Property	Cell A	Cell B
Nominal Capacity (mAh)	90	120
Nominal Voltage (V)	3.7	3.7
Operating Temperature (charging) (°C)	0 to 45	0 to 45
Operating Temperature (discharging) (°C)	-20 to 60	-20 to 60

TABLE I. PHYSICAL PROPERTIES OF TEST VEHICLES

Battery charging has been done using a constant current-constant voltage (CCCV) charge profile, while battery discharging has been done using a constant current profile. The properties of both cells' charge-discharge profiles as given by the manufacturers are listed in TABLE II:

Property	Cell A	Cell B
End of Charge Voltage (V)	4.2	4.2
Charge Current Range (mA)	45 (0.5C) to 180 (2C)	60 (0.5C) to 240 (2C)
End of Charge Current (mA)	1.7	2.4
End of Discharge Voltage (V)	3	3

TABLE II. CHARGE-DISCHARGE CHARACTERISTICS OF TEST VEHICLES

B. *Testing Setup and Methodology*

The experimental process and equipment developed at Auburn University's NSF-CAVE3 Electronics Research Center [14]**Error! Reference source not found.** were used in this study.

Fig. 1 displays the schematic diagram of the accelerated life cycling setup. A power management integrated circuit (PMIC), and an electronic load were alternately connected to the battery terminals through a relay board to perform the CC-CV (constant current-constant voltage) charging and CC discharge processes for the li-ion battery. The voltage at the battery terminals is measured by the data acquisition system (DAQ), and the battery current by a current sensor. The life cycling test is automated by the LabVIEW code. Data is recorded by the DAQ, saved by the code, and processed in MATLAB to determine battery capacity and degradation. Following are the two quantities that were processed for analysis (battery capacity (Q) and SOH (see (2) and (3))):

$$Q = \sum_{t=0}^{t=end} (I_{discharge} \times t_{sampling}) \tag{2}$$

$$SOH = \frac{Q_{n^{th}\ cycle}}{Q_{rated}} \tag{3}$$

The sampling interval for computing battery capacity (Q) varies from 6s to 1200s and its effect on SOH estimation will be discussed further.

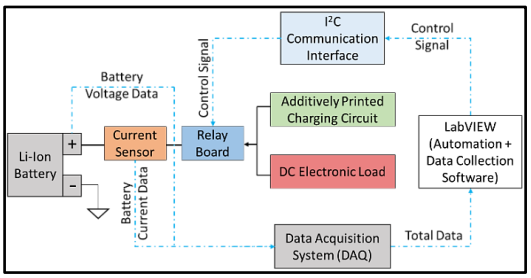

Fig. 1: Test setup for accelerated life cycling of power sources

The randomized testing format has three variations:

(i) Randomized depth of cycling
(ii) Randomized C-rate cycling
(iii) Combined randomized cycling

Randomized depth of cycling, and randomized C-rate test cases are implemented using modified LabVIEW codes. The upper and lower bounds of SOC are first established for the randomized depth of cycling test, and SOC is then randomly varied for each discharge and charge cycle in increments of 10%. Four levels of SOC bounds: 0 – 100%, 60 – 100%, 0 – 40%, and 30 – 70% have been chosen for conducting the randomized depth of cycling test to emulate users who operate devices in different SOC ranges. The code has been designed such that, in all testing scenarios, the battery would never go below 0% SOC or rise over 100% SOC (see Fig. 2).

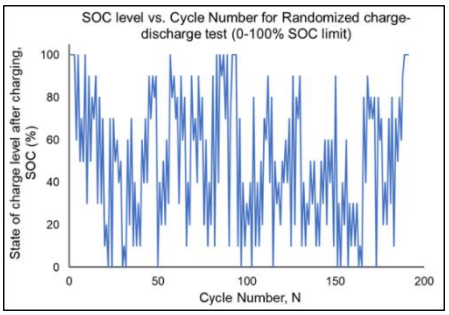

(A)

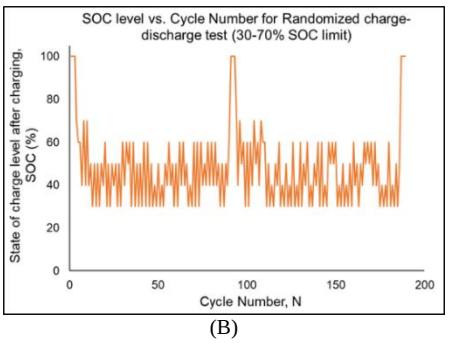

(B)

Fig. 2. State of charge variation for Randomized depth of cycling test. SOC bounds: (A) 0 – 100%, (B) 30 – 70%

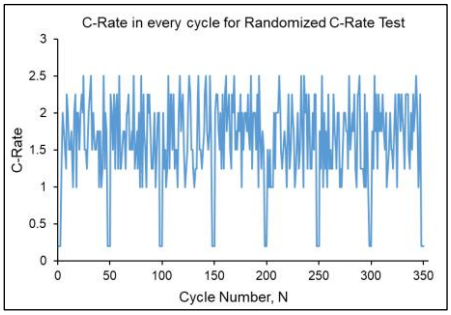

Fig. 3. C-rate variation vs. Cycle Number for Randomized C-Rate Test

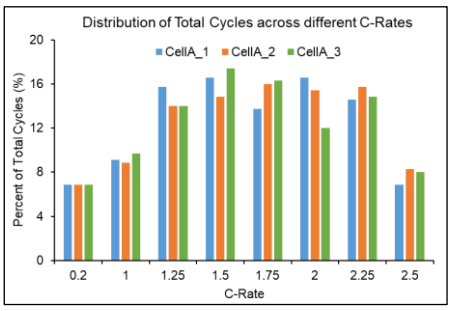

Fig. 4. Distribution of C-rates across cycles for three randomized C-rate tests

The randomized C-rate cycling scenario was added to demonstrate the robustness of the estimation model although it doesn't exactly represent a battery use-case. C-rates ranging from 1C to 2.5C are provided as input in the LabVIEW code for the randomized C-rate testing. Then, one C-rate is picked for charging from the provided list before each charging cycle (see Fig. 3 and Fig. 4). Both randomizing techniques are used simultaneously in combined randomized cycling. After every

50 cycles of randomized cycles, 3 full cycles at 0.2C C-rate are conducted to measure the full capacity of the battery.

C. Test Matrix

Use-parameter	Levels
C-Rate	1.5C, 1.75C, 2C
Depth of Charge/ Discharge	50%, 75%, 100%
Operating Temperature	25 °C, 40 °C

TABLE III. FIXED-DEPTH BATTERY TESTING USE PARAMETERS AND LEVELS USED FOR MODEL TRAINING DATA

Test Type	SOC lower/upper bounds	C-Rate
Randomized Depth of Cycling	0 – 100%	1.5C
	60 – 100%	
	0 – 40%	
	30 – 70%	
Randomized C-Rate	0 – 100%	1C – 2.5C
Combined Cycling	0 – 100%	1C – 2.5C
	60 – 100%	
	0 – 40%	
	30 – 70%	

TABLE IV. RANDOMIZED-DEPTH AND RANDOMIZED C-RATE CYCLING TEST MATRIX USED FOR MODEL TESTING DATA

The test matrices used in this study are presented in this section. The numerous use parameters and their values employed for accelerated life cycling of batteries used for model training are shown in TABLE III. This training data's development was documented in [14]. The levels of the individual variables provided in this test matrix have been maintained constant across various cycles for each test. The tests run using the training data combine numerous levels of each use-parameter in different tests. A total of 19 tests were used as the training data for cell A and 12 tests for cell B.

The test matrix for the battery samples that were used as the testing data for the created model is shown in TABLE IV with each test case being repeated with three samples.

III. RESULTS AND DISCUSSION

A. Regression Model Development

The model created for this study is an update of the model provided in Lall [15] (see (4(4)). The earlier model links the normalized cycle number (N), the C-rate (C), the battery operating temperature (T), and the integrated voltage (IV) to the battery SOH. It was trained using fixed charge current and fixed depth of cycling data. To effectively predict the SOH for the randomized depth of cycle and charge current data, the model must be modified.

$$SOH = 100 - b_1 N^{b_2} C^{b_3} e^{b_4(\frac{1}{298}-\frac{1}{T})} IV^{b_5} \tag{4}$$

As the battery is charged/discharged within different SOC bounds during each cycle, making each cycle inconsistent with the preceding one, the cycle number has an uncountable nature in a randomized cycling scenario. Therefore, cumulative integrated voltage (CIV), which is the cumulative integral of the battery voltage w.r.t. time over the course of the battery's cycling, has been used in place of 'cycle number (N)' (see (5)).

$$CIV_i = \int_{N=1}^{N=i} V dt \tag{5}$$

The battery voltage range for a partial cycle differs from that for a deep cycle. As a result, CIV precisely depicts the depth of cycling that the battery sample has sustained. Furthermore, the older model had a power law equation, whereas the newer model has been modified to have a two-term exponential model equation. The two term exponential model fits battery degradation curves closely, as the battery capacity fade is a two-phase decay process [15][16]. The new model keeps the C-rate variable in its current form. The operating temperature variable has been considered as a ratio with 298 K (ambient). The prior model, which was normalized to 100% SOH at the first cycle, was created to compare the degradation accrued due to various levels of use-parameters. However, the new model has been developed for non-normalized SOH data in order to estimate the SOH in scenarios from the real world. Consequently, battery's SOH at the first cycle (SOH_0) was included as a variable. Lastly, the 'cumulative averaged voltage' variable represents the average SOC that the battery runs at (see (6)). Either the charge phase ($V_i^{avg,charge}$) (Model 1 (7)) or the discharge phase ($V_i^{avg,discharge}$) (Model 2 (8)) can be used as a variable. As a result, the new SOH estimation model has been updated and two variants have been proposed:

$$V_i^{avg,charge} = \frac{\sum_{N=1}^{N=i} (\overline{V_{N=i}^{charge}})}{i} \tag{6}$$

Model Variant 1:

$$SOH = b_1 (SOH_0)^{b_2} C^{b_3} (\frac{T}{298})^{b_4} (\frac{V_{avg,charge}}{4.2})^{b_5} (e^{b_6 * CIV} + b_7 e^{b_8 * CIV}) \tag{7}$$

Model Variant 2:

$$SOH = b_1 (SOH_0)^{b_2} C^{b_3} (\frac{T}{298})^{b_4} (\frac{V_{avg,discharge}}{4.2})^{b_5} (e^{b_6 * CIV} + b_7 e^{b_8 * CIV}) \tag{8}$$

Furthermore, like CIV, a cumulatively integrated current (CIC) variable, defined in (9), can also be used to generate two more model variants ((10) and (11)):

$$CIC = \int_{N=0}^{N=i} I dt \tag{9}$$

Model Variant 3:

$$SOH = b_1 (SOH_0)^{b_2} C^{b_3} (\frac{T}{298})^{b_4} (\frac{V_{avg,charge}}{4.2})^{b_5} (e^{b_6 * CIC} + b_7 e^{b_8 * CIC}) \tag{10}$$

Model Variant 4:

$$SOH = b_1(SOH_0)^{b_2} C^{b_3} (\frac{T}{298})^{b_4} (\frac{V_{avg,discharge}}{4.2})^{b_5} (e^{b_6 * CIC} + b_7 e^{b_8 * CIC}) \quad (11)$$

The four model equations listed above have been used to generate exclusive models for both cells A and B, wherein each exclusive model has been trained using the data of only one cell type and has been used to estimate the SOH for randomized tests of that particular cell. In the 'Exclusively Cell B' model, operating temperature has not been considered as a variable owing to the knee-point failure observed at 40°C [14]. Moreover, two types of combined models have been developed, which have been trained using the data for both cells and have been tested on randomized tests for both cells. The first type of combined model is the 'Capacity Agnostic Model' which doesn't include battery capacity as a variable (same equation as (*7*, (*8*, (*10*, (*11*); whereas the second type is the 'Capacity Conscious Model' which includes the battery capacity as a variable (see (12)). Thus, a total of four model types (2 exclusive, 2 combined) have been developed in this study, each with four model variants as described earlier.

$$SOH = b_1(SOH_0)^{b_2} C^{b_3} (\frac{T}{298})^{b_4} (\frac{V_{avg,charge}}{4.2})^{b_5} (e^{b_6 * CIV} + b_7 e^{b_8 * CIV})(\frac{Cap}{100})^{b_9} \quad (12)$$

The memory and processing power needed for data sampling and subsequent estimation is another practical concern when using SOH estimation models in real-world devices. The amount of memory used by the device increases as the data sampling rate increases. Eight different data sampling rates were used on the training/ testing datasets as a fix for this issue. The sampling intervals were: 6s, 18s, 30s, 60s, 120s, 300s, 600s and 1200s. As a result, in the 18-second scenario, the voltage and current datapoints in the entire training dataset will be sampled every 18 seconds, and the resulting sampled dataset will be utilized to compute CIV/ V_i^{avg} and then train the model. The same process will be applied to the randomized datasets for model testing. Thus, a total of 128 SOH estimation models—4 model types, 4 variants with different variables, and 8 sub-variants with different sampling intervals—were developed and will be compared in the sections that follow.

B. SOH Estimation Error across Cycle Numbers

Results for the validation of the SOH estimation models against the randomized depth of cycling, randomized C-rate, and combined randomized testing data are presented in this section.

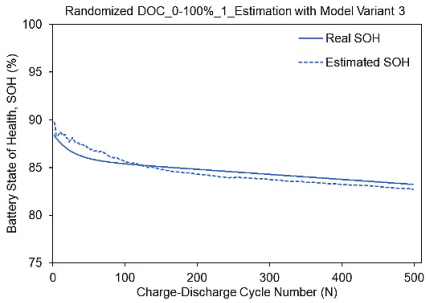

(A)

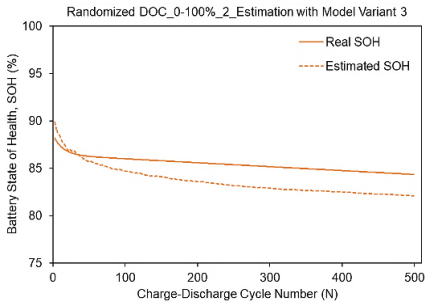

(B)

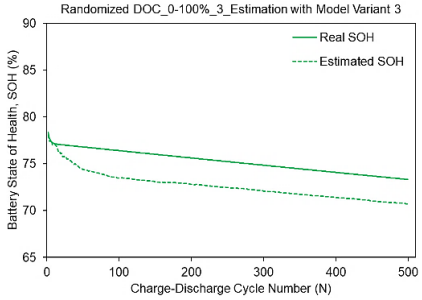

(C)

Fig. 5. Real vs Estimation State of Health for Randomized Depth of Cycling Test for Cell A, (A) Sample 1, (B) Sample 2, (C) Sample 3

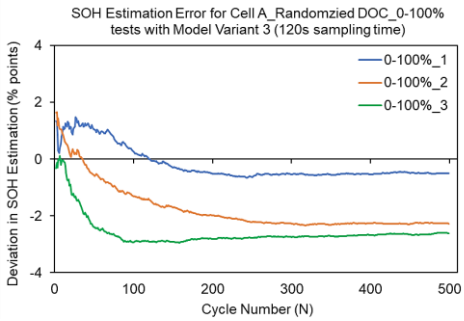

Fig. 6. Error in SOH Estimation for Cell A: Randomized Depth of Cycling Test (all three samples)

Fig. 5 shows the real vs estimated SOH plots for the three samples of the randomized depth of cycling test for cell A within the bounds 0 – 100% for model variant 3 with 120s sampling interval. The test type and model conditions chosen for Fig. 5 are for representative purposes since plotting the entire dataset in this manner would be expansive and repetitive. Fig. 6 shows the error in SOH estimation, i.e. the difference between real and estimated SOH for the same three tests. The

SOH estimation error for all the three samples for the same test case has been averaged and has been presented in Fig. 7 (A) with error bars along with similar datapoints for tests with 60-100%, 0-40%, and 30-70% SOC bounds. It can be seen that for the four test types with different SOC bounds, the average SOH estimation errors are in the range, +2 to -3% points. The SOH estimation error is positive in initial cycles and becomes negative as the cycle number increases, due to the nature of the real and estimated SOH curves as seen in Fig. 5.

Fig. 7 (B) and (C) are plots similar to Fig. 7 (A), but for randomized C-rate cycling, and combined randomized cycling scenarios. For these cases too, the model variant 3 with 120s sampling interval results in error values between +2 to -4% points. For comparing the estimation performance across model variants and subvariants, the SOH estimation error across cycles was computed into a single value via root mean square averaging presented further.

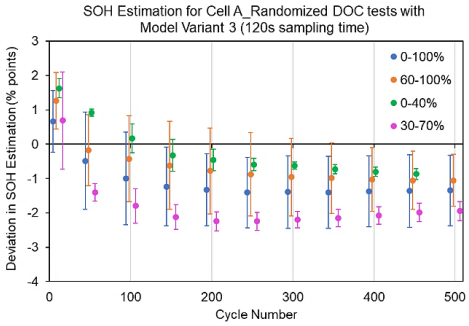

(A)

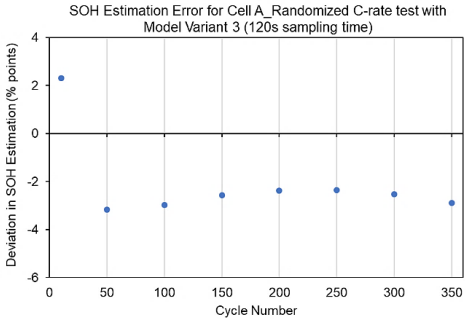

(B)

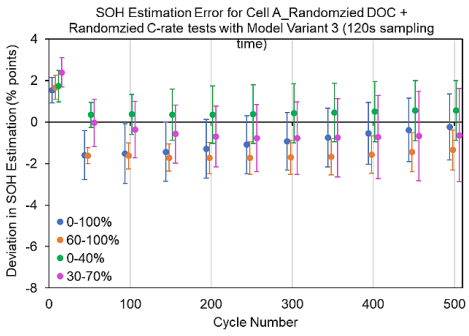

(C)

Fig. 7. SOH Estimation Error for Cell A for all SoC bounds, (A) Randomized Depth of Cycling, (B) Randomized C-Rate, (C) Randomized Depth of Cycling + Randomized C-Rate

C. Exclusively Cell A/ Cell B Model

This section presents the results RMS error in SOH estimation for all variants and sub-variants of the 'Exclusively Cell A' model for all the test cases. TABLE V enlists the coding for the X-axis legend used for the comparison graphs listed throughout the results and discussion section.

Sr. No.	Test condition
1_0-100	Random DOC 0-100%
1_60-100	Random DOC 60-100%
1_0-40	Random DOC 0-40%
1_30-70	Random DOC 30-70%
2	Random C-Rate
3_0-100	Combined Cycling Test 0 – 100%
3_60-100	Combined Cycling Test 60 – 100%
3_0-40	Combined Cycling Test 0 – 40%
3_30-70	Combined Cycling Test 30 – 70%

TABLE V.X-AXIS LEGEND FOR FIGURES IN SECTION III

Fig. 8 (A) (B) (C) (D) are root mean square error (RMSE) graphs corresponding to the model variants 1, 2, 3, and 4 respectively. In each sub-figure, there are nine bar clusters, one for each test type listed as per TABLE V. Finally, each bar cluster comprises of eight bars corresponding to 8 sub-variants as listed in the sub-figure legend. The color of bars getting lighter (pale blue) to darker (black) from left to right indicates an increase in the sampling interval from 6s to 1200s.

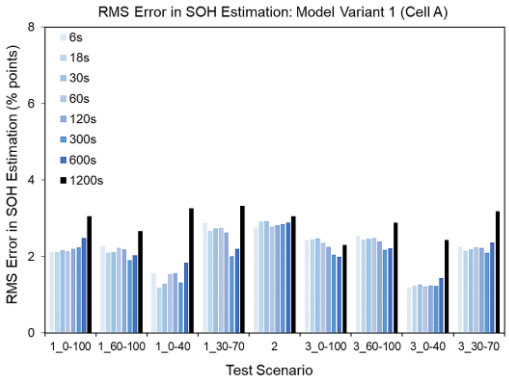

(A)

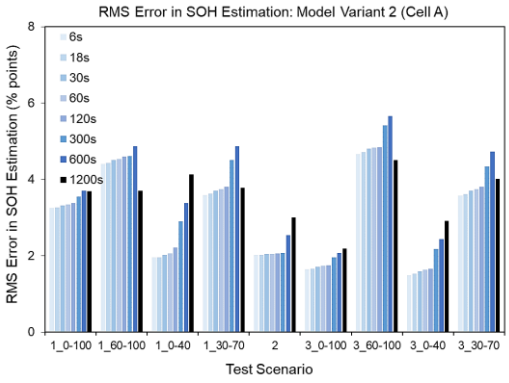

(B)

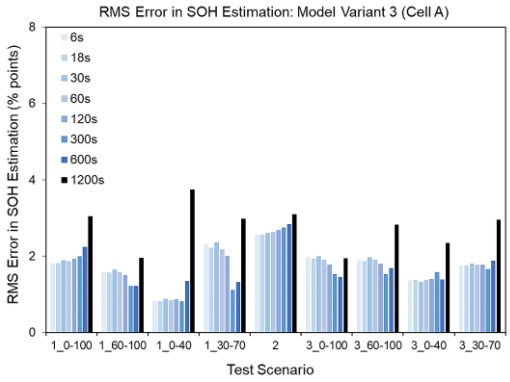

(C)

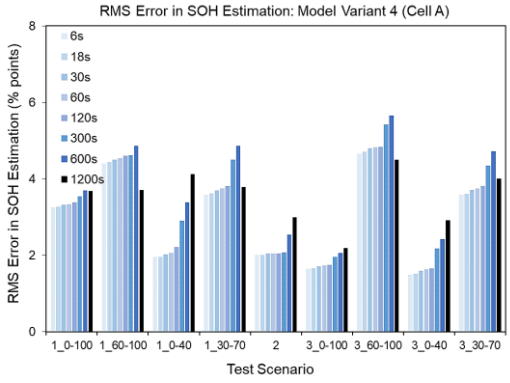

(D)

Fig. 8. Comparison of RMS SOH Estimation Error for Exclusively Cell A Model for all sampling intervals and test cases. (A) Model Variant 1, (B) Variant 2, (C) Variant 3, (D) Variant 4.

As can be seen in Fig. 8, as the sampling interval increases, the RMSE in SOH estimation increases, due to the variables CIVi and V_i^{avg} being computed with sparser datapoints, thereby reducing their accuracy of being correlated with battery SOH. Significant rise in RMSEs can be noted once the sampling interval increases beyond 300s. Fig. 9 and Fig. 10 depict the variation of CIV and V_i^{avg} with cycle number for different sampling intervals. For higher sampling times, with increasing cycle number, the CIV increases slowly, thereby lowering its correlation with progressive life cycling, i.e. SOH degradation. In Fig. 10, the V_i^{avg} value reduces with increasing sampling intervals. This is because, the battery majorly operates in the voltage range of 3.7 – 4 V, and due to lower sampling intervals, the cumulative average of the voltage skews more towards a value between 3.7 – 4 V. Thus, this skewing process results in similar V_i^{avg} values for different test types, which makes them indistinguishable in a regression model. Thus, as a compromise between lower computational intensiveness and acceptable estimation RMSE, a 120s sampling interval was chosen as a representative of each test case/ model variant.

Furthermore, model variants 1 and 3 register a lower RMSE as compared to variants 2 and 4. Model variants 1 and 3 use $V_i^{avg,charge}$ as opposed to variants 2 and 4 which use $V_i^{avg,discharge}$ as a variable to represent the average voltage at which the battery operates, i.e., the average operation SOC. Fig. 11 compares the $V_i^{avg,charge}$ and $V_i^{avg,discharge}$ values for all training tests of cell A. It can be seen that $V_i^{avg,charge}$ varies over a larger voltage range than $V_i^{avg,discharge}$. Thus, $V_i^{avg,charge}$ would be better correlated with battery SOH as opposed to $V_i^{avg,discharge}$ for different test types, which would explain the higher accuracy of variants 1 and 3 over variants 2 and 4.

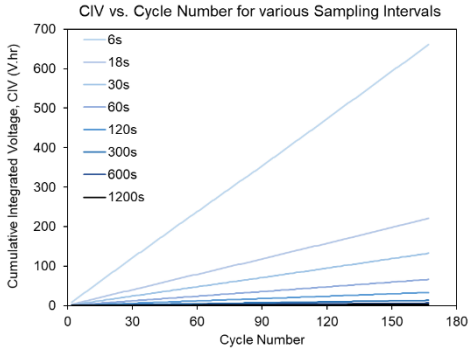

Fig. 9. Cumulative integrated voltage vs. cycle number for various sampling intervals

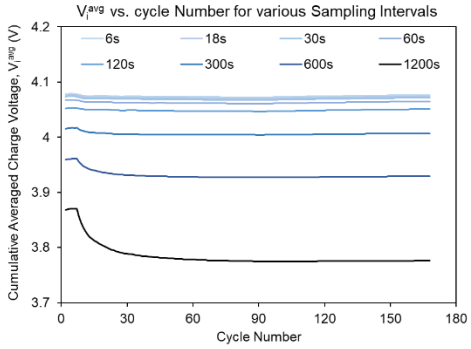

Fig. 10. Cumulative averaged charge voltage vs. cycle number for various sampling intervals

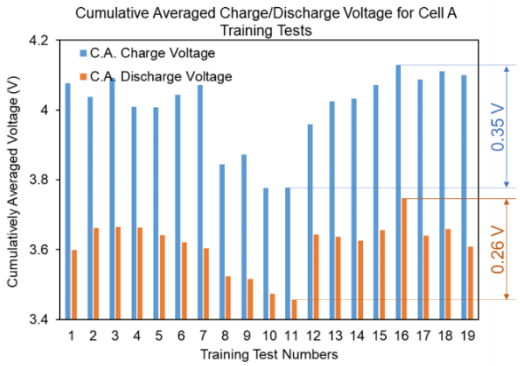

Fig. 11. Comparison of cumulative averaged charge and discharge voltage for Cell A training tests

Fig. 12 summarizes the RMSE results for four variants of the exclusively cell A model for 120s sampling time for all the test cases.

Similar trends are observed for the exclusively cell B model as seen in Fig. 13. The exclusively cell B model has a lower estimation RMSE than cell A owing to a higher R-squared of the trained regression model. This difference could be because the training dataset for cell B excludes tests

performed at 40°C and the exclusively cell B model excludes operating temperature as a variable.

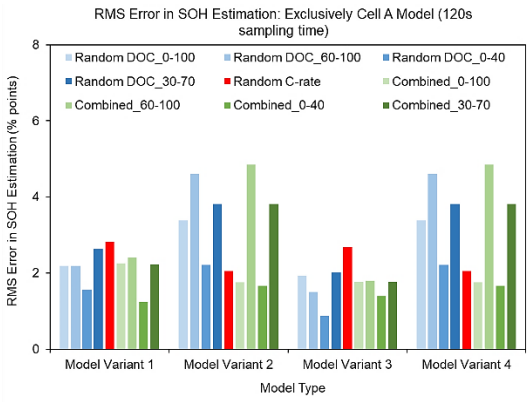

Fig. 12. Comparison of RMS SOH Estimation Error for all variants of Exclusively Cell A Model for 120s sampling interval for all test cases

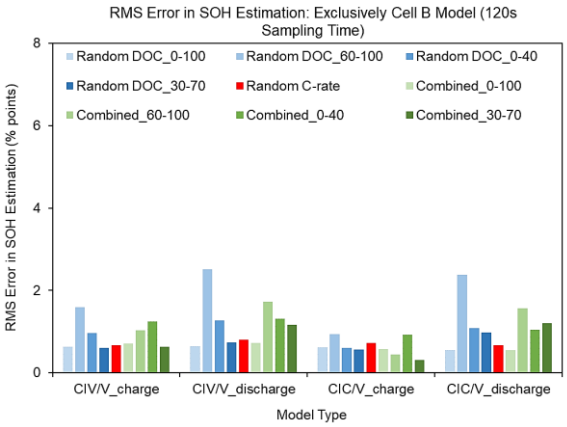

Fig. 13. Comparison of RMS SOH Estimation Error for all variants of Exclusively Cell B Model for 120s sampling interval for all test cases

D. Capacity Agnostic and Capacity Conscious Models

Fig. 14 shows RMSE results for the capacity agnostic model for all four variants for 120s sampling time for all test cases (A) cell A, and (B) cell B. All the trends explained previously for variant comparison can be seen here as well. Another peculiarity observed here is that, in Fig. 12, Fig. 13, and Fig. 14, the RMSE for randomized depth of cycling and combined cycling tests with the SOC bounds 60-100% is higher compared to the other test cases for model variants 2 and 4. Tis is because, model variants 2 and 4 include $V_i^{avg,discharge}$ as the variable to represent the average battery SOC which is within the range 3.5 – 3.75 V as seen in Fig. 11. However, for tests with SOC bounds 60-100%, the battery voltage is often greater than 3.8 V for the entire duration of battery cycling. Thus, due to a V_i^{avg} value outside the ones experienced during model training, model variants 2 and 4 result in a higher RMSE for tests with SOC bounds 60-100%. However, since the range for $V_i^{avg,charge}$ is greater than that for $V_i^{avg,discharge}$, model variants 1 and 3 that are trained using $V_i^{avg,charge}$ do not experience a similar high error for low SOC test cases (SOC bounds 0-40%). Fig. 15 shows similar plots as Fig. 14, but for the capacity conscious model.

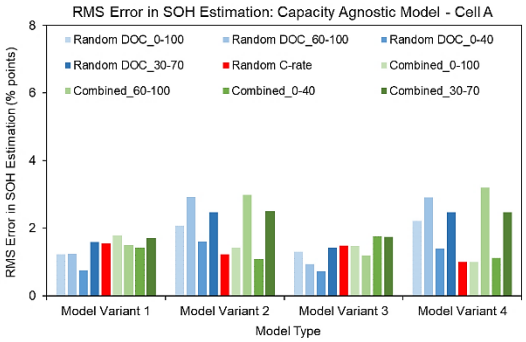

(A)

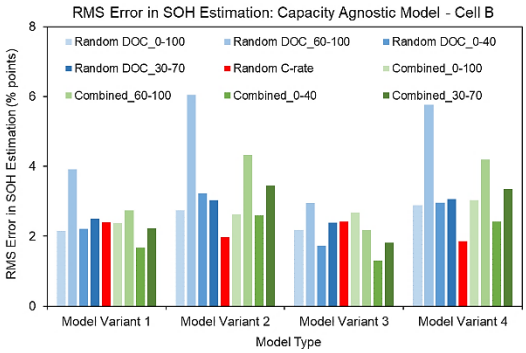

(B)

Fig. 14. Comparison of RMS SOH Estimation Error for all variants of Capacity Agnostic Model for 120s sampling interval for all test cases. (A) Cell A, (B) Cell B

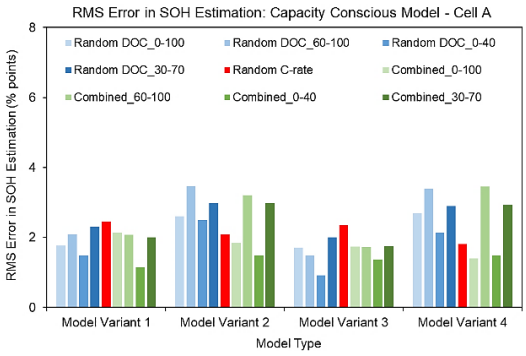

(A)

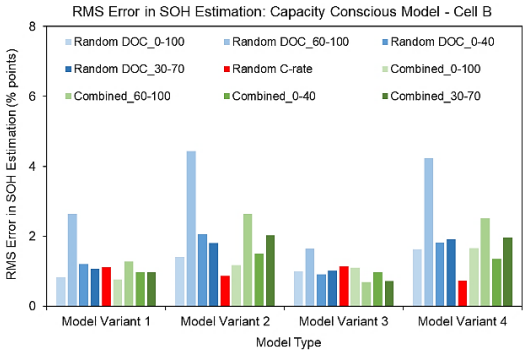

(B)

Fig. 15. Comparison of RMS SOH Estimation Error for all variants of Capacity Conscious Model for 120s sampling interval for all test cases. (A) Cell A, (B) Cell B

E. *Comparison of Exclusive and Combined Models*

This section compares all model types and established model variants for both the cells A and B. As discussed before, model variants 1 and 3 perform better than variants 2 and 4, and would hence be chosen for comparison between model types. Fig. 16 compares estimation RMSE amongst the three model types for cell A: exclusively cell A, capacity agnostic, and capacity conscious models. The average RMSEs computed for different test cases are listed for each model type/ variant in both sub-figures of Fig. 16. Upon comparison of the average RMSE values, it can be seen that the model variant 3 performs marginally better than the variant 1. Furthermore, all three model types perform similarly for cell A with the capacity agnostic model registering the lowest average RMSE.

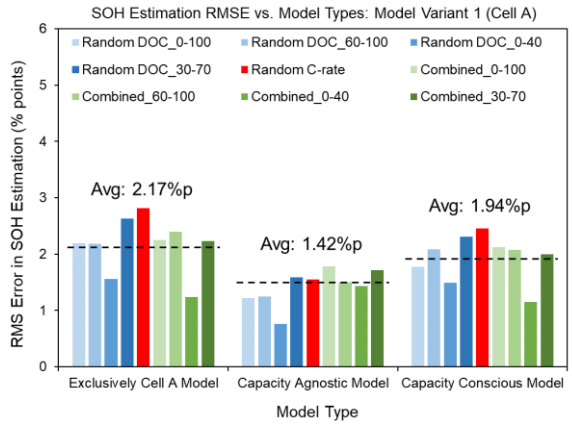

(A)

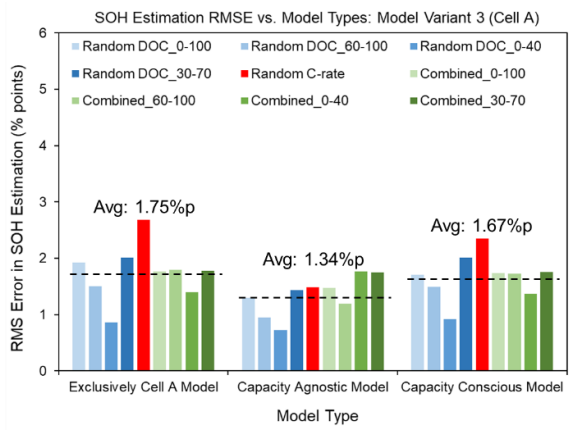

(B)

Fig. 16. Comparison of RMS SOH Estimation Error for all test cases across 3 model types for Cell A for 120s sampling time. (A) Model Variant 1, (B) Variant 3

Fig. 17 shows a similar graph as Fig. 16, but for cell B. Here too, the model variant 3 marginally outperforms variant 1. However, a peculiar trend in RMSE values is seen here among the three model types. The capacity conscious model for cell B registers almost the same RMSE value as the exclusively cell B model, whereas the capacity agnostic model shows a very high RMSE as compared to the other two model types. The reasoning behind this will be discussed further.

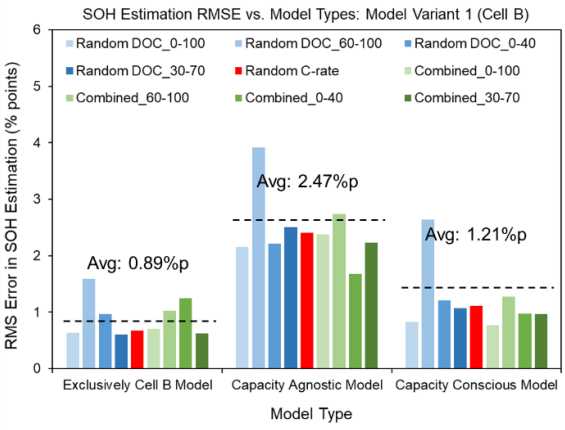

(A)

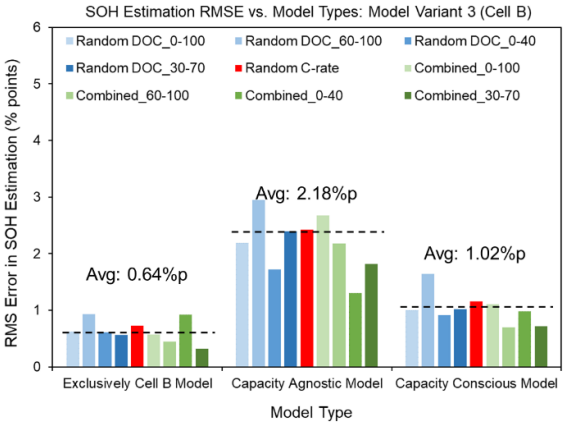

(B)

Fig. 17. Comparison of RMS SOH Estimation Error for all test cases across 3 model types for Cell B for 120s sampling time. (A) Model Variant 1, (B) Variant 3

Firstly, the capacity agnostic model has been trained using the 19 datasets for cell A and 12 datasets for cell B. Moreover, the capacity agnostic model excludes the capacity variable, and hence, the model cannot distinguish whether the provided data belongs to cell A or cell B. Owing to this, and the fact that the model has been trained on higher number of datasets for cell A, it might be skewed towards cell A more resulting in a higher estimation accuracy for cell A as compared to that for cell B.

On the other hand, the capacity conscious model has been trained on the same datasets as the capacity agnostic model, but includes the battery capacity as a variable which helps it distinguish between data from both cells. As a result, the model accuracy of the capacity conscious model is similar to those of the exclusive cell models for both the cells.

Thus, from the plethora of models explored in this study, the most applicable model with low error for both the cells would be the capacity conscious model with variant 3 and with a sampling interval of 120s as listed here (13):

$$SOH = 0.53(SOH_0)^{1.13} C^{-5E-3} \left(\frac{T}{298}\right)^{0.34} \left(\frac{V_{avg,charge}}{4.2}\right)^{-0.39} \left(e^{-29.34*\left(\frac{CIC}{10^6}\right)} + 0.03e^{-7524.3*\left(\frac{CIC}{10^6}\right)}\right)\left(\frac{Cap}{100}\right)^{0.1} \quad (13)$$

IV. SUMMARY AND CONCLUSION

The training of multiple SOH estimation models for two coin cells using fixed depth of cycling datasets, as well as the testing of these models on randomized depth of cycling, randomized C-rate, and combined randomized cycling datasets, have all been successfully demonstrated in this study. For the randomized depth of cycling of the battery samples, four distinct SOC bounds were selected, and the C-rates for randomized C-rate tests ranged from 1C to 2.5C. In addition, four model variants were devised with different variable combinations. For each model variant, eight sub-variants with different sampling times were also examined. Furthermore, two combined models for both the coin cell types were developed and compared to the exclusive models. We came at the following conclusions from the model validation process: (1) The model accuracy is high at low sampling intervals, but suffers at sampling intervals >300s, making 120s interval a good compromise between high accuracy and low computational intensiveness. (2) For all the three randomized test types: the estimation performance observed was uniform or similar, except for certain model types and sampling intervals. (3) Model variants 1 and 3 performed significantly better than model variants 2 and 4 owing to the wider range of the cumulatively averaged charge voltage variable used in variants 1 and 3. (4) Among the combined models, the capacity agnostic model performs better for cell A than cell B owing to the model training data being skewed due to the higher number of cell A training datasets. (5) The capacity conscious model includes the battery capacity as a variable due to which it performs with similar accuracy for both cell A and cell B as their respective exclusive models. Thus, the methodology presented in the current paper is able to train a SOH estimation model from fixed-depth of cycling data (as generated in a laboratory setting) and the developed model is able to estimate the SOH of randomly cycled batteries in various topologies, to imitate the battery usage in the real world, with an error under 3% points.

ACKNOWLEDGMENT

The research results presented in this paper have been supported by members of NSF-CAVE3 Electronics Research Center.

REFERENCES

[1] G. Zhou, F. Li, H. Cheng, “Progress in flexible lithium batteries and future prospects,” *Energy Environ. Sci.*, vol. 7, no. 4, pp. 1307-1338, 2014.

[2] J.D. MacKenzie, C. Ho, “Perspectives on energy storage for flexible electronic systems,” *Proc. IEEE*, vol. 103, no. 4, pp. 535-553, 2015.

[3] Y. Wang, B. Liu, Q. Li, S. Cartmell, S. Ferrara, Z.D. Deng, J. Xiao, “Lithium and lithium ion batteries for applications in microelectronic devices: A review,” *J. Power Sources*, vol. 286, pp. 330–345, 2015.

[4] X. Luo, J. Wang, M. Dooner, and J. Clarke, “Overview of current development in electrical energy storage technologies and the application potential in power system operation,” *Appl. Energy*, vol. 137, pp. 511–536, 2015.

[5] M. Aneke, M. Wang, “Energy storage technologies and real life applications – A state of the art review,” *Appl. Energy*, vol. 179, pp. 350-377, 2016.

[6] N. Nitta, F. Wu, J. T. Lee, and G. Yushin, “Li-ion battery materials: present and future,” *Mater. today*, vol. 18, no. 5, pp. 252–264, 2015.

[7] G. Zubi, R. Dufo-López, M. Carvalho, and G. Pasaoglu, “The lithium-ion battery: State of the art and future perspectives,” *Renew. Sustain. Energy Rev.*, vol. 89, no. April 2017, pp. 292–308, 2018.

[8] Y. Li, K. Liu, A.M. Foley, A. Zulke, M. Berecibar et al., “Data-driven health estimation and lifetime prediction of lithium-ion batteries: A review,” Renew. Sust. Energ. Rev., vol. 113, October 2019.

[9] B. Bole, C. Kulkarni, M. Daigle, “Randomized battery usage data set,” In NASA AMES Prognostics Data Repository; NASA Ames Research Center: Moffett Field, CA, USA, 2014.

[10] J. Yu, B. Mo, D. Tang, J. Yang, J. Wan, J. Liu, “Indirect State-of-Health Estimation for Lithium-Ion Batteries under Randomized Use,” *Energies*, vol. 10, no. 12, 2017.

[11] P. Venugopal, T. V., “State-of-Health Estimation of Li-ion Batteries in Electric Vehicle Using IndRNN under Variable Load Condition,” *Energies*, vol. 12, no. 22, 2021.

[12] H. Tian, P. Qin, “State of health prediction for lithium-ion batteries with a novel online sequential extreme learning machine method,” *Int J Energy Res.*, 2021.

[13] N. Yang, Z. Song, H. Hoffmann, J. Sun, “Robust state of health estimation of lithium-ion batteries using convolutional neural network and random forest,” *J Energy Storage*, vol. 48, 2022.

[14] P. Lall, V. Soni, G. Sethi, K. Yiang, “SOH modeling of Li-ion coin cells subjected to varying C-rates, depths of charge, operating temperatures and custom charge profiles,” *IEEE ITherm 2021,* Virtual, Online. June 1–4, 2021.

[15] S.F. Schuster, T. Bach, E. Fleder, J. Muller, M. Brand *et al.*, “Nonlinear aging characteristics of lithium-ion cells under different operatinal conditions,” J. Energy Storage, vol. 1, pp.44-53, June 2015.

[16] P. Ma, S. Wang, L. Zhao, M. Pecht, et. al., “An improved exponential model for predicting the remaining useful life of lithium-ion batteries,” *IEEE ICPHM 2015*, Austin, Texas, USA. 22 – 25 June 2015.